Economic Geology, v. 105, pp. 339–349

Conditions for Early Cretaceous Emerald Formation at Dyakou, China: Fluid Inclusion, Ar-Ar, and Stable Isotope Studies

G. Xue,[1] D. Marshall,[1,†] S. Zhang,[2] T. D. Ullrich,[3] T. Bishop,[1] L. A. Groat,[3]
D. J. Thorkelson,[1] G. Giuliani,[4] and A. E. Fallick[5]

[1]*Department of Earth Sciences, Simon Fraser University, Burnaby, British Columbia V5A 1S6, Canada*

[2]*Department of Earth Sciences, Science and Technology University of Kunming, Kunming, Yunnan 650093, China*

[3]*Department of Earth and Ocean Sciences, University of British Columbia, Vancouver, British Columbia V6T 1Z4, Canada*

[4]*Centre de Recherches Pétrographiques et Géochimiques-CNRS, BP 20, 54501 Vandeouvre-Cedex, France*

[5]*Isotope Geoscience Unit, SURRC, East Kilbride Glasgow, G75 OQF, Scotland*

Abstract

The Dyakou emerald occurrence is located in Malipo County in the province of Yunnan, southern China. The occurrence lies in the northern part of the Laojunshan-Song Chay metamorphic core complex, which is exposed in an area of approximately 2,000 km^2 and extends across the border between China and Vietnam. Emerald mineralization is hosted by pegmatite and associated quartz veins that intrude deformed Proterozoic biotite-muscovite granofels and schist. Hydrogen and oxygen isotope results from the emerald channel waters and emerald, respectively, are consistent with an igneous fluid source. The $\delta^{18}O$ fractionation between emerald and quartz yields vein temperatures of 365° to 420°C. Fluid inclusions indicate that the emerald precipitated from saline brines ranging from almost pure water to 10.5 mass percent NaCl equiv. Fluid inclusion isochores intersected with $\delta^{18}O$ data yield pressures changing along the geothermal gradient from 1,500 to 3,300 bars. Ar-Ar geochronology of biotite and muscovite from the emerald veins yields consistent ages of 124 ± 1 Ma. These constraints combined with field observations indicate that the Dyakou emerald deposit is consistent with the igneous-related model for emerald formation.

Introduction

Beryl and its green, chromium-vanadium–rich variety, emerald, typically contain abundant fluid inclusions. Pioneering work by Roedder (1963, 1972, 1982) on fluid inclusions in emerald led to a better understanding of pressures, temperatures, and fluid conditions responsible for emerald precipitation. Ed Roedder's studies indicated a diverse range of fluid compositions and modes of origin, most notably the hypersaline fluids associated with some emeralds and a diverse range of daughter and accidental crystals, all of which could be used to differentiate between natural and synthetic gems. In this paper, we examine fluid inclusions from the Dyakou emerald occurrence in Malipo County, southeastern Yunnan, China. Our work builds on preliminary fluid inclusion studies by Zhang et al. (1999) and Moroz et al. (2004) on samples from Dyakou, which indicated brine and rare brine-CO_2 fluid inclusion assemblages similar to those in fluid inclusions from other emerald occurrences documented by Roedder (1963, 1972, 1982).

In 1992, prospectors discovered gem-quality emerald crystals near Dyakou village while exploring for tungsten (Fig. 1). It is the only significant emerald discovery in China. Previous geologic work in the vicinity of the Dyakou showing included geologic mapping at 1:10,000 scale by Wang et al. (1996) and at 1:50,000 scale by Feng et al. (1998). In 1996, emerald produced from the area was officially named the "Chinese emerald" by the Yunnan Geological Survey. Summaries of data from the mapping projects pertaining to the emerald mineralization are published in Zhang et al. (1998, 1999), Feng et al. (2000), and Lu et al. (2001).

The relative rarity of emerald worldwide can partially be explained by low Be concentrations in Earth's crust and generally higher concentrations in pegmatite, clays, black shale, and their metamorphic equivalents such as gneiss and mica schist. Be is the least abundant of the first 40 elements on the periodic table with an average crustal concentration of less than 5 ppm (Wedepohl, 1978). In contrast, Cr (±V) is most commonly enriched in mafic and ultramafic rocks in geologic environments incongruous with Be. Therefore, unusual geologic and geochemical conditions are required to bring Be and Cr together to form emerald (Schwarz et al., 2002). Two general models for emerald precipitation proposed by Schwarz and Giuliani (2001) are widely accepted: a granite-related model and a tectonic-hydrothermal model. In the first model, granitic to pegmatitic rocks intrude Cr (±V)-rich host rocks, introducing Be and heat into the mineralization system. In the second model, emerald formation results from a Be-rich fluid flowing through major crustal faults and shear zones and interacting with Cr (±V)-rich metamorphic rocks at upper greenschist to lower amphibolite facies. This study characterizes the Dyakou emerald occurrence as a granite-related emerald deposit, using fluid inclusion, stable and radiogenic isotope studies.

Regional Geology

The Dyakou emerald showing occurs in the northern part of the Laojunshan-Song Chay metamorphic core complex (Fig. 1). The exposure of the Laojunshan-Song Chay is more than 2,000 km^2 and extends across the China-Vietnam border,

† Corresponding author: e-mail, marshall@sfu.ca

Submitted:October17, 2008
Accepted: October17, 2009

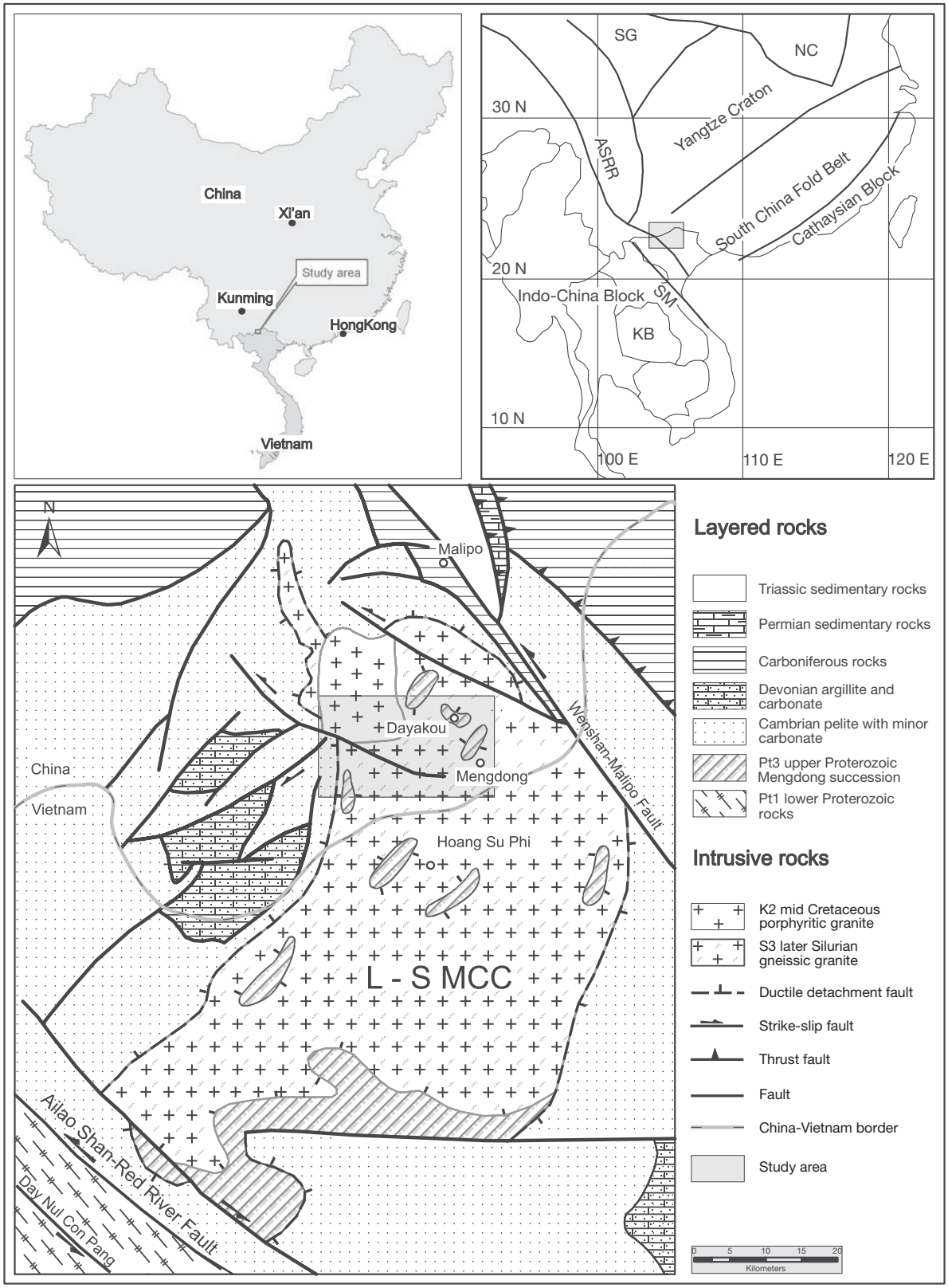

FIG. 1. Regional geologic map, showing the major lithologic units in the study area. The index map (inset upper left) shows the location of the study area. The tectonic map (inset upper right) shows the study area (rectangle) relative to the larger scale tectonic setting (after Feng et al., 2000; Roger et al., 2000). Abbreviations: ASRR = Ailao Shan-Red River fault, KB = Korat basin, L-S MCC = Laojunshan-Shay Metamorphic Core Complex, NC = North China-Korea block, SG = Song pan Garze, SM = Song Ma suture.

and is the largest core complex in the southeastern South China block (Li et al., 1996; Zhang et al., 1998; Roger et al., 2000; Maluski et al., 2001; Liu et al., 2003, 2006). The Dyakou emerald occurence is northeast of the northwest-southeast–trending Ailaoshan-Red River shear zone that separates the South China and Cathaysia blocks from the Indochina block. Major left-lateral ductile shearing occurred along this zone during the Oligo-Miocene as Indochina was transported several hundreds of kilometers toward the southeast (Tapponnier et al., 1986, 1990; Yang and Besse, 1993; Leloup et al., 1995; Roger et al., 2000). The emerald occurrence is bounded in the northeast by the Wenshan-Malipo strike-slip faults that were active beginning in the Early Devonian.

The Laojunshan-Song Chay metamorphic core complex consists of a weakly metamorphosed cover that is structurally detached from a more highly metamorphosed core (Zhang et al., 1998; Roger et al., 2000; Liu et al., 2006; Yan et al., 2006). The cover consists of Cambrian and Devonian slate, phyllite, mica schist, and marble with metamorphic grades ranging from lower greenschist grade at the core to lower grades in more distal locations. These metasedimentary rocks were derived from mud rock and carbonate. The core is dominantly composed of migmatite, granite, and laminated and augen gneiss derived from the metamorphism and deformation of Caledonian to Cathaysian (ca. 400–140 Ma) granites. Remnant patches of the Precambrian Mengdong succession are situated locally within the core. The nucleus has been intruded by Cretaceous porphyritic granites in the northwestern part of the complex. Cover and core are separated by extensional shear zones with both ductile and brittle character. These structures denuded the cover and led to exhumation of the core.

Zhang et al. (1998) divided the Mengdong succession into two units based on their lithology, deformation, and metamorphism: the Nanyantian (Pt3n) and Saxi (Pt3s). In sheared contact with gneisses, the Nanyantian unit is generally composed of schist. Overlying the Nanyantian unit, the Saxi unit is comprised of granofels, gneiss, amphibolites, and calcareous sediementary rocks. Ductile shear zones separating different lithologic layers are common and occur at different scales. Other structures include intrafolial folds, sheath folds, C-S fabrics, and boudins. Liu et al. (2006) reported Neoproterozoic (U-Pb zircon) ages of 761 ± 12 and 829 ± 10 Ma from two igneous units within the plagioclase-rich gneiss of the Nanyantian unit. These dates may be related to the breakup of the supercontinent Rodinia. Inherited 1.83 Ga zircons within the Nanyantian imply the existence of the paleo-Proterozoic basement in the South China block (Li et al., 2002a, b; Liu et al., 2006).

The regional metamorphic grade attained by the Mengdong succession is lower amphibolite facies (Lu et al., 2001). Based on garnet-biotite (Hodges and Spear, 1982) and garnet-biotite-plagioclase (Hoisch, 1991) thermobarometers, the regional P-T conditions were estimated, using garnet mica schist, at 550° to 580°C and 4.5 to 6 kbars (Roger et al., 2000). However, the same garnet-biotite thermometer suggested a temperature in the range of 550° to 680°C using samples from a garnet mica schist (Lu et al., 2001). In addition, Feng et al. (1998) reported that a sample of amphibolite yielded a pressure of approximately 5 kbars, using the relationship between Al^{vi} and Si in hornblende (Raase, 1974).

Local Geology

In the vicinity of the Dyakou emerald occurrence, the Proterozoic Mengdong succession consists mostly of structurally layered metamorphic rocks (Fig. 2). The basal unit within this succession is the Nanyantian schist (Pt3n), which generally comprises biotite + muscovite schist and biotite + muscovite quartz schist in sheared contact with Late Silurian gneissic granite. According to Wang et al. (1996), the overlying rocks to the foliated Nanyantian unit is the Saxi unit (Pt3s) consisting of biotite granofels with several lenses of plagioclase amphibolite (Pt3s-1), striped biotite granofels and plagioclase gneiss with minor biotite-muscovite schist (Pt3s-2), and epidosite, quartzite, and tremolite plagioclase granofels (Pt3s-3). The granofels with granoblastic texture in the Saxi unit is the only host rock for emerald mineralization in the Dyakou occurrence. The Saxi unit consists of quartz (30–60%), orthoclase (15%), plagioclase (25–60%), biotite (10%), and minor tourmaline, sphene, apatite, and pyrite.

The Late Silurian gneissic biotite + plagioclase + orthoclase granite (S-type) is the dominant igneous rock in the area. Zircon from the gneissic granite has been dated at 411 Ma using U-Pb (Feng et al., 1998). Nearly 1 km south of the emerald showing, the gneissic granite is intruded by an apophysis of Late Cretaceous porphyritic (S-type) granite, which is dated by Ar-Ar at 76 Ma (Feng et al., 2000).

Emerald at the Dyakou showing is found mainly in northwest-southeast quartz veins (Fig. 3) paralleling the foliation plane in the Saxi unit, and northeast-southwest–trending felsic pegmatite veins (Fig. 4) dipping 15° to 30° toward northnorthwest and crosscutting the Proterozoic Mengdong succession. The pegmatite crosscuts the quartz veins indicating at least two main episodes of emerald mineralization. Typically, emeralds within the pegmatite veins are more abundant and are more idiomorphic than emeralds associated with the quartz veins. In contrast, emeralds associated with quartz veins in shear zones are less abundant but higher quality (Wang et al., 1996). Some pegmatite veins display local zoning with an outermost orthoclase zone followed by an inner quartz zone, and an emerald-rich zone in the middle of the vein. Twenty-two pegmatite and eight quartz veins have been documented with an estimated reserve of approximately 7 tons of emerald crystals (Wang et al., 1996).

The pegmatite and quartz veins are similar in their mineralogy but have different modal abundances. This relationship is similar to the emerald occurrence in Yukon Canada, with an observed gradation from dominantly pegmatitic veins to dominantly quartz veins (Groat et al., 2005). The major minerals are quartz (75–90%) and potassic feldspar in both vein types, with minor variable amounts of mica (phlogopite, muscovite, or fuchsite). These veins also contain minor amounts of tourmaline, scheelite, fluorite, and calcite. Sulfide such as pyrrhotite, pyrite, and arsenopyrite are also present (Zhang et al., 1999).

Fluid Inclusions

Previous fluid inclusion studies at Dyakou identified a dominant fluid inclusion type of two-phase (brine + vapor)

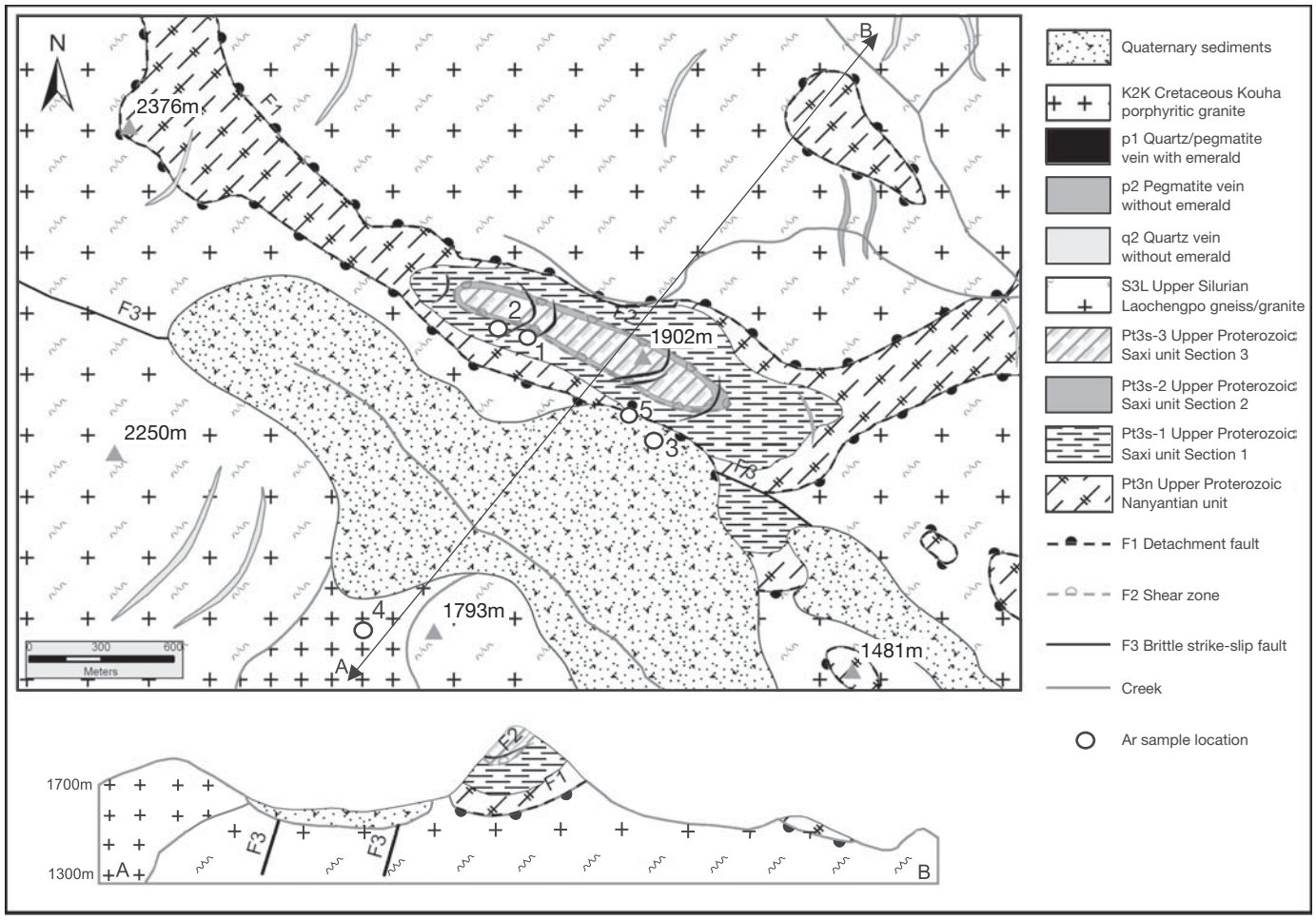

FIG. 2. Geologic map of the Dyakou emerald occurrence (after Wang et al., 1996). The cross section (A-B) illustrates the tectonic layering in the area.

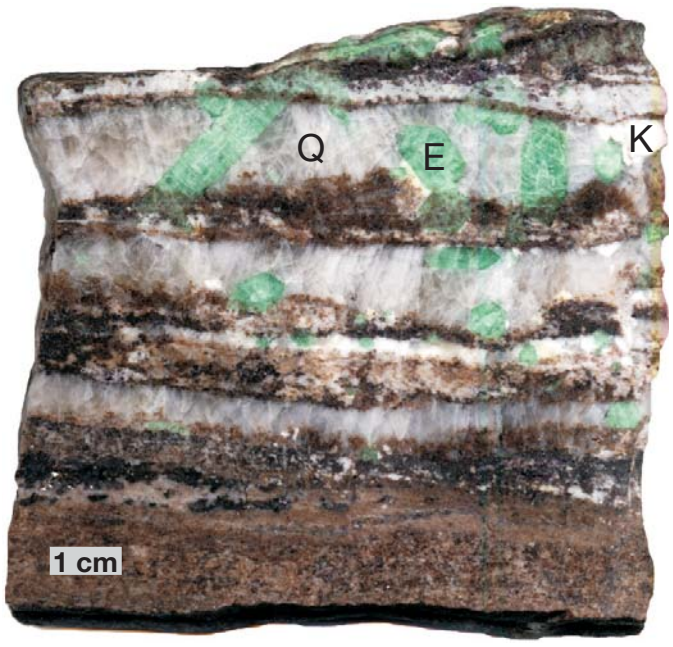

fluid inclusions (Zhang et al., 1999; Moroz et al., 2004) and a very rare brine-CO_2 fluid inclusion type (Zhang et al., 1999). Only the brine-vapor fluid inclusion type was identified in this study. The fluid inclusions occur within most of the transparent vein minerals and were measured in quartz, emerald, and fluorite. The fluid inclusions are abundant within quartz and emerald and range in size from submicroscopic to 25 μm. Most inclusions occur along trails of healed fractures or more rarely as isolated inclusions. The fluid inclusions were grouped into distinct fluid inclusion assemblages based on observable timing relationships between individual fluid inclusions (Goldstein and Reynolds, 1994; Bodnar, 2003). At room temperature the inclusions contain approximately 85 vol percent brine and approximately 15 vol percent vapor.

FIG. 3. Emerald-bearing quartz vein comprised of quartz (Q), emerald (E), and minor potassic feldspar (K). Multiple laminae of host schist within the vein displaying crack-seal–like texture are dominantly recrystallized to quartz, feldspar, and minor phlogopite. Specimen DYK06-zh.

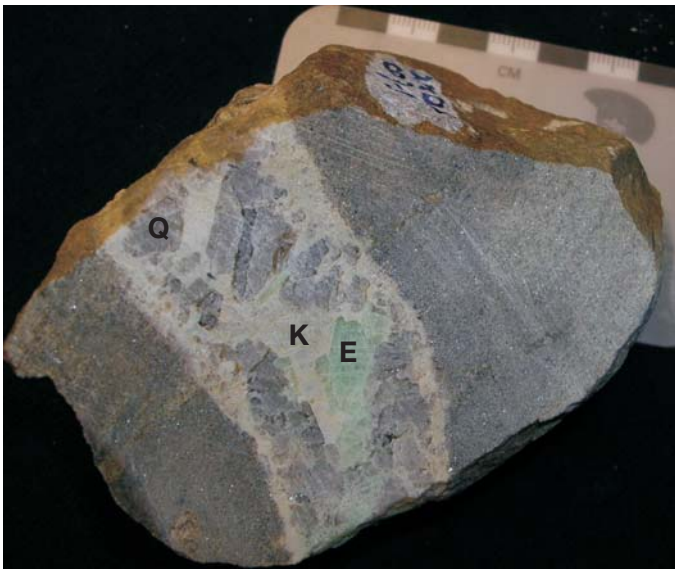

FIG. 4. Emerald-bearing pegmatitic vein comprised of quartz (Q), potassic feldspar (K), and emerald (E). The host rock is a foliated phlogopite schist of the Proterozoic Saxi unit. The minerals within the vein show no evidence of deformation, while the biotite in the host rock defines a vein-parallel foliation. Specimen DYK06-007.

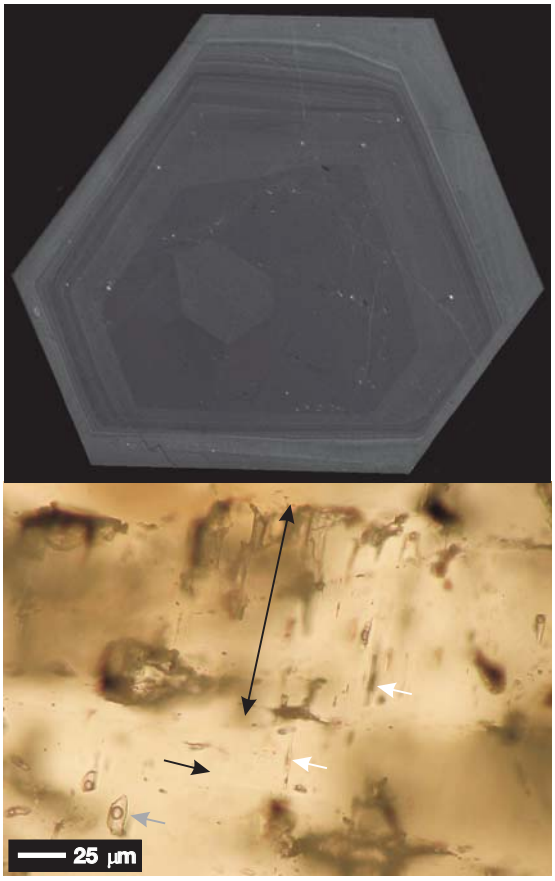

FIG. 5. Top photo shows a cathode luminescence SEM image of a 1-mm emerald crystal displaying multiple fine-scale growth zones defined by sharp as well as nonlinear boundaries. The bottom photomicrograph shows typical two-phase (liquid + vapor) fluid inclusions (gray arrow) in emerald. Similar growth zone textures such as nonlinear growth zones (double arrow) defined by abundant large fluid inclusions, typical growth zone perpendicular fluid inclusions (white arrows), and very fine scale growth zones (black arrow) are observed in doubly polished emerald plates. Specimen DYK05-2B: Squashed frog chip.

The emerald and quartz display faint growth zones in transmitted light. These zones are generally defined by areas of more abundant versus less abundant fluid inclusions, fine-scale optical banding, and growth-zone–perpendicular-elongate fluid inclusions. The growth zoning is more easily observed as finely layered concentric cathode-luminescent active zones within idiomorphic emerald (Fig. 5). The growth zones are also distinguished chemically based on Na, Mg, and V concentrations. Thus the dominant fluid inclusion type is considered to be contemporaneous with the emerald and other vein minerals, based on the petrographic relationships between growth zones and fluid inclusions, the overall abundance of these fluid inclusions, the petrographic equilibrium observed between all the emerald-bearing vein minerals, and the lack of any other fluid inclusion types within the vein minerals. Samples were chosen from both the emerald-bearing pegmatitic and quartz veins. There is no observable difference in the fluid inclusions from the individual vein types (or host minerals) on the basis of petrography.

Microthermometry

Upon rapid cooling, the two-phase fluid inclusions nucleate ice at temperatures between –30° and –60°C. Upon further cooling to –190°C, no other phase changes were observed. Heating the fluid inclusions from –190°C results in the first melting of the ice at temperatures ranging from –10° to –30°C. These elevated first melting temperatures are likely due to the optics in the tiny inclusions inhibiting recognition of the small amounts of melts present at eutectic temperatures. Likewise, the minor depression of the NaCl-H_2O eutectic temperatures indicates there may be other divalent cations such as Ca or Mg present at relatively low concentrations. Continued heating results in ice melting temperatures over the temperature range –0.1° to –7.0°C. The ice melting temperatures correspond to salinities ranging from 0.2 to 10.5 mass percent NaCl equiv (Bodnar, 1993). Further heating decreases the volume of the vapor bubble until final homogenization of the fluid inclusion contents into the liquid phase occurs over a temperature range of 204° to 280°C. Some inclusions decrepitated or stretched upon heating. These data were not used in the study.

Salinity differences in quartz and emerald-hosted fluid inclusions

A plot of the total homogenization temperature versus ice melting temperature reveals a scattered but relatively flat trend (Fig. 6), which indicates a range of salinities over relatively constant temperatures. However, there is a noticeable separation in the salinities between fluid inclusions hosted in quartz and those hosted in emerald. The inclusions hosted in quartz have salinities ranging from 0 to approximately 5.5 wt percent NaCl equiv, the inclusions hosted within emerald tend to have higher salinities ranging from approximately 5.5 to 9 wt percent NaCl equiv. Another 20 fluid inclusions from the same samples that could not be petrographically classified

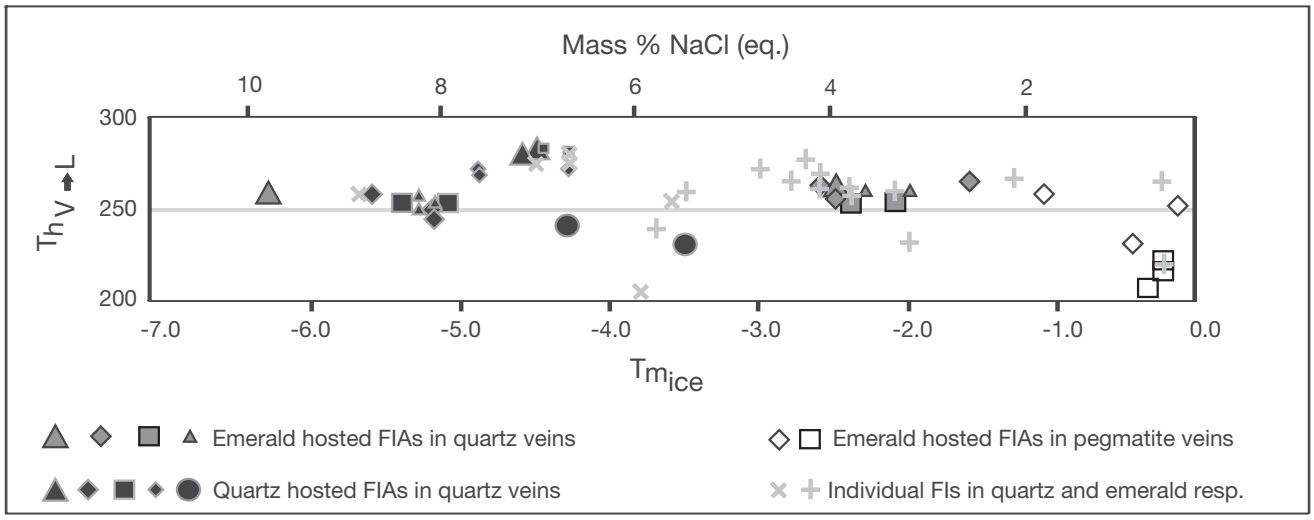

FIG. 6. Total homogenization (T_h) vs. ice-melting (T_m) temperature diagram for fluid inclusions hosted within emerald and quartz from the Dyakou emerald veins. All filled symbol types relate fluid inclusions within the same fluid inclusion assemblage (FIA). The white-filled symbols represent inclusions hosted in emerald from the pegmatite veins. The gray-filled symbols are inclusions hosted within emerald from the quartz veins and black-filled symbols are inclusions hosted within quartz from the quartz veins. The light-gray cross and X symbols represent individual fluid inclusions from emerald and quartz, respectively.

into fluid inclusion assemblages show a less distinct but similar trend (Fig. 6).

Ar-Ar Geochronology

Five samples were selected for ^{40}Ar-^{39}Ar dating to determine the age of emerald mineralization and to determine if any of the local metamorphic and igneous rocks were related to emerald formation. Samples were crushed and sieved and the 100- to 200-μm-size fraction was handpicked to ensure pure mineral separates. Table 1 lists the Ar-Ar age determinations for the related geologic units in the Dyakou region. All the spectra yielded geologically interpretable plateau ages (Fig. 7).

Muscovite and biotite from the emerald-bearing quartz and pegmatite veins, respectively, show similar ages at approximately 124 Ma. Muscovite from the emerald-bearing quartz vein yielded an age plateau at 124.27 ± 0.70 Ma based on 72.5 percent of the total ^{39}Ar released (Fig. 7). Biotite from an emerald-bearing pegmatite vein yielded a plateau based on 61.5 percent of the ^{39}Ar released consistent with an age of 123.78 ± 0.67 Ma. The consistency in the ages between the two emerald-bearing vein types is consistent with the veins being genetically related and also indicates that the veins are older than the original Late Cretaceous age first proposed by Zhang et al. (1999).

TABLE 1. $^{40}Ar/^{39}Ar$ Ages from the Dyakou Emerald Occurrence

Ar sample no.	Specimen no.	Rock type	Age ± 2σ (Ma)	Plateau ^{39}Ar %
1	DYK07-05	Ms-quartz vein	124.27 ± 0.70	72.5
2	DYK06-03	Bt-pegmatite vein	123.78 ± 0.67	61.5
3	DYK06-08-2	Bt-S3l (Laochengpo intrusion)	119.38 ± 0.65	62.2
4	DYK06-09	Bt- K2k (Kohua intrusion)	64.40 ± 0.45	78.6
5	DYK06-13	Bt-Pt3s (Saxi granofels)	103.20 ± 0.54	85.1

Three other rocks in the study area were also selected for Ar-Ar dating. These were the Proterozoic Saxi granofels, which is the host to the emerald veins, and two local granitic rocks; the Silurian Laochengpo granite and the Cretaceous Kouha intrusion. Either of the granitic units may have been a heat and/or Be source for the emerald veins. The youngest of the granitic rocks, the Kouha granite yielded an early Tertiary age of 64.40 ± 0.45 Ma (Fig. 7). The Kouha has been dated in a number of localities and yielded diverse Cretaceous ages including 75 and 93 to 118 Ma using Ar-Ar (Feng et al., 1998), 93 Ma using Rb-Sr (Feng et al., 1998), 88 and 94 Ma using U-Pb zircon (Liu et al., 2006), and 86 and 146 Ma (Yan et al., 2006) also using U-Pb zircon. This range of Cretaceous dates is consistent with an interval of protracted Cretaceous plutonism in the region and although the Kouha granite postdates emerald emplacement, it is deemed most probable that one of the other nearby intrusions related to the protacted Cretaceous plutonism is related to the circa 124 Ma emerald vein emplacement.

The Proterozoic Saxi granofels and the Silurian Laochengpo granitic unit yielded Ar-Ar ages of 103.20 ± 0.54 and 119.38 ± 0.65 Ma, respectively. Both of these ages are too young and inconsistent with other ages and geologic constraints (Feng et al., 1998; Roger et al., 2000; Maluski et al., 2001; Yan et al., 2006; Liu et al., 2006) for these units and are interpreted as resetting ages during the protracted period of Cretaceous plutonism within the area.

Thus the relative timing of different events in the study area are consistent with some degree of Ar resetting during the Cretaceous for the pre-Cretaceous Saxi granofels and the Laochengpo granitic rocks, while the Cretaceous emerald

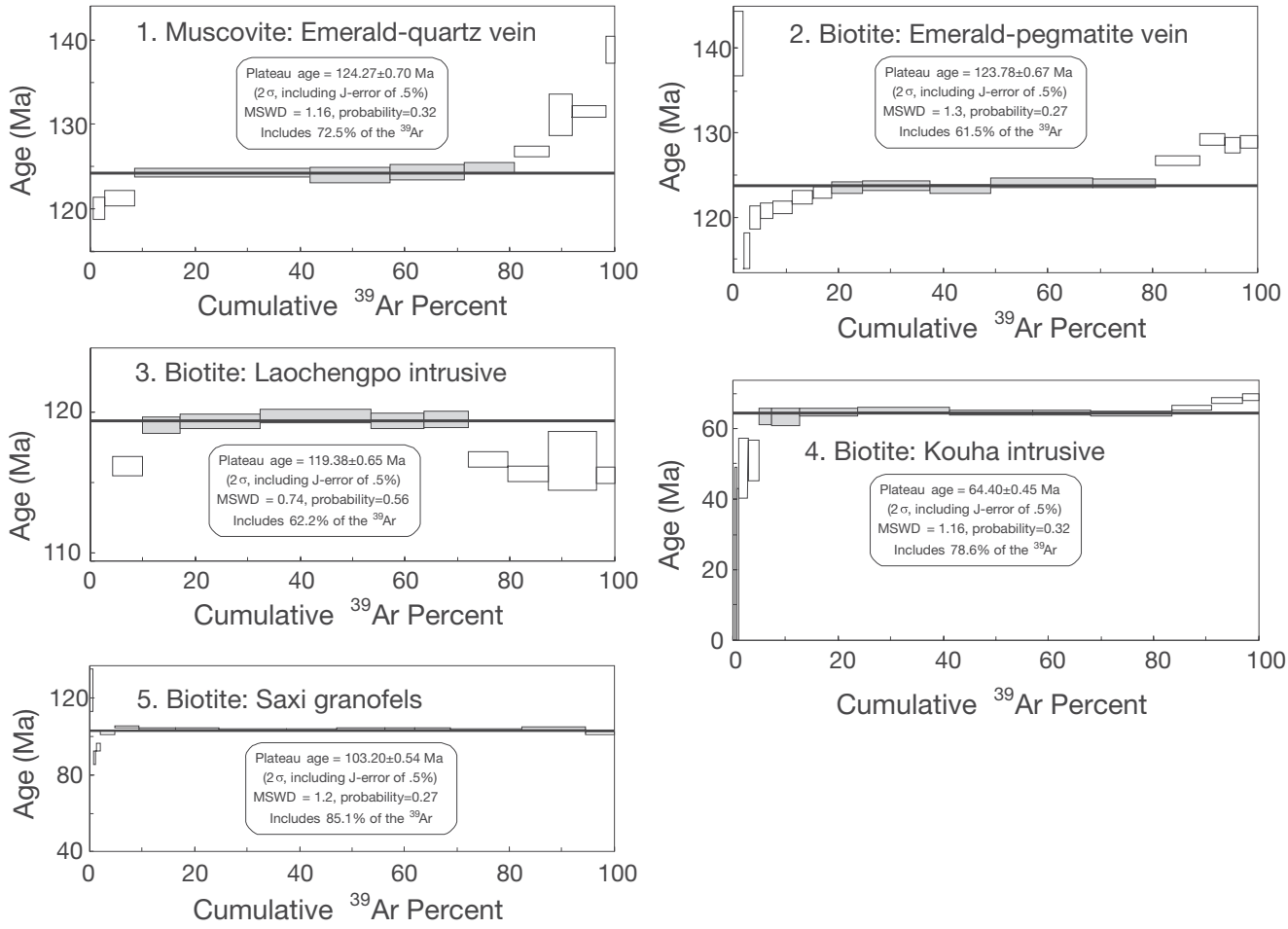

FIG. 7. Five ^{40}Ar-^{39}Ar gas release spectra showing plateau ages ranging from Early Cretaceous to early Tertiary. The plateau ages are shown as a black line across each individual spectrum. Laser heating steps used in the calculation of the plateau ages are shown in gray. All errors are shown at the 2 level. Sample numbers (1–5) correspond to the Ar sample locations in Figure 2. The older ages observed in the high-temperature release portions of the spectra for samples 1, 2, and 4 are interpreted as Ar recoil.

veins yield geologic interpretable plateau ages consistent with emerald deposition occurring at approximately 124 Ma as part of the protracted Cretaceous plutonism. Lastly, the Ar-Ar signatures of the emerald veins show no disturbance from the intrusion of the early Tertiary Kouha granite, as it was intruded at shallow crustal levels and is sufficiently distant from the emerald veins to minimize any metamorphic aureole effects.

Geochemistry

Whole-rock geochemical data can be used to determine possible sources of Be and Cr (±V) in emerald deposits. The emerald from Dyakou is V dominant but has a range of V/Cr from 6 to 3, with V_2O_3 and Cr_2O_3 concentrations ranging up to 0.65 and 0.16 wt percent, respectively. The whole-rock data for all the geologic units in the Dyakou emerald occurrence are given in Table 2. The Be content of the pegmatite vein is 12 ppm. This concentration is relatively low but still in excess of crustal abundances of Be of less than 5 ppm according to Wedepohl (1978) or less than 3.5 ppm as listed by Beus (1966). The Paleocene porphyroid granite listed in Table 2 contains the highest concentrations of Be (34.7 ppm) but the ^{40}Ar-^{39}Ar age indicates that it postdates the Dyakou emerald veins. Thus the Paleocene granites could not have been the source of the Be for the Dyakou emerald. The more probably Be sources are other granitic plutons within the protracted Cretaceous plutonism within the area.

The rocks with the highest concentrations of Cr (±V) in the study area are the metamorphic rocks of the Mengdong succession; most specifically, the Saxi unit has the highest concentrations of Cr (±V) and is always host to the emerald-bearing veins at Dyakou. Thus the Saxi unit is deemed the most likely source of Cr (±V) for the Dyakou emerald.

Stable Isotopes

Beryl crystallizes in the hexagonal system and is composed of interconnected six-membered rings of silica tetrahedra. This arrangement produces channels parallel to the c-axis, which are large enough to accommodate a range of fluids and dissolved cations that maintain charge balance within the beryl. The fluids trapped within the channel contribute minimally to the overall $\delta^{18}O$ values of the beryl host but, more

TABLE 2. Whole-Rock Geochemical Data for the Major Rock Types in the Study Area

(%)[1]	SiO_2	Al_2O_3	Fe_2O_3	CaO	MgO	Na_2O	K_2O	Cr_2O_3	TiO_2	MnO	P_2O_5	SrO	BaO	LOI	Total
1	87.32	6.69	0.67	1.49	0.15	1.38	0.72	<0.01	<0.01	<0.01	0.01	0.03	0.47	0.24	99.17
2	57.46	19.89	1.46	3.93	1.54	7.05	2.09	0.01	0.19	0.08	0.37	0.1	0.56	3.41	98.15
3	49.00	15.82	13.15	9.13	4.79	3.46	0.71	0.03	2.59	0.27	0.68	0.03	0.06	0.25	99.97
4	65.57	12.47	7.41	2.4	1.09	2.58	2.94	0.02	0.71	0.02	0.21	0.04	1.55	1.71	98.72
5	55.76	7.77	6.66	4.71	17.07	0.13	3.45	<0.01	0.14	0.21	0.01	<0.01	0.13	2.49	98.53
6	74.31	12.92	2.14	0.72	0.23	3.04	4.97	0.01	0.17	0.02	0.04	0.01	0.02	0.32	98.92
7	71.59	16.87	0.86	0.05	0.11	3.76	4.07	<0.01	<0.01	0.03	0.36	<0.01	0.01	2.26	99.97
(ppm)	Be	Cr	V	W	Eu	Lu	Ba	Ga	Zr	P	Rb	Sr	Sn	Y	U
1	7	10	130	352	0.13	0.1	3770	10.7	8	10	78.7	31	58	11.3	1.3
2	**12.1**	50	**732**	1720	0.62	0.82	4520	22.6	74	1930	218	92	81	59.8	2.55
3	<0.5	**100**	**215**	13	2.89	0.79	492	21.1	263	3300	25.6	16	3	56.5	1.57
4	0.9	**90**	**276**	13	1.37	0.54	>10000	12.3	214	1010	144.5	20	47	43.9	43.9
5	2.6	10	**517**	3	0.19	0.28	1155	23.4	10	40	262	1	9	22.3	0.74
6	0.7	10	12	39	0.57	1.4	163	21.4	185	130	580	3	17	84.9	24.3
7	**34.7**	10	<5	18	0.06	0.06	28.1	31.4	33	1020	1570	5	218	4.6	7.23

[1] 1= quartz vein, 2 = beryl-bearing pegmatite, 3 = amphibolite (Pt3S), 4 = granofels (Pt3S), 5 = schist (Pt3N), 6 = Late Silurian gneissic granite, 7 = Paleocene porphyroid granite

importantly, contain the only hydrogen within the beryl structure and represent the original formational fluid in equilibrium with the beryl during crystallization (Taylor et al., 1992). Extraction and trapping of the channel fluids above 800°C and subsequent δD analyses have been used in conjunction with $\delta^{18}O$ analyses of the beryl to distinguish between different emerald deposits, determine fluid source and deposit type (Giuliani et al., 1997). Hydrogen and oxygen stable isotope ratios (Table 3) from emerald at Dyakou are consistent with the δD-$\delta^{18}O$ signature of highly evolved peraluminous granitic rocks (Fig. 8) with a possible minor contribution from the host metamorphic rocks.

Thermometry derived from existing $\delta^{18}O$ partitioning between the quartz and emerald in the emerald veins using the calibrations of Taylor et al. (1992) and Zheng (1993) yield unrealistically high temperatures of greater than 700° and 900°C, respectively. This is a consistent problem worldwide for emerald deposits and we propose a very preliminary empirical calibration for quartz -beryl ^{18}O partitioning based on the few points available from emerald occurrences with published ^{18}O data and corresponding depositional temperatures (Arif et al., 1996; Groat et al., 2002; Marshall et al., 2003;). The temperatures derived for emeralds described in these papers are independent of the beryl ^{18}O compositions and derived from mineral equilibria or other isotopic thermometers. These data are consistent with the following ^{18}O fractionation values:

$$1000\ Ln\alpha_{qtz\text{–}beryl} = \left(\frac{1.153 * 10^6}{T^2}\right) - 0.81 \qquad T \text{ in Kelvin}$$

Using this empirically derived equation, the measured $\delta^{18}O$ quartz-beryl fractionations from the Dyakou emerald occurrence (Table 3) are consistent with temperatures in the range 365° to 420°C. These temperatures are consistent with observed level of wall-rock alteration and metamorphism surrounding the veins and are similar to other emerald-pegmatite occurrences.

Pressure-Temperature Fluid Conditions

A relatively complete picture of pressure-temperature fluid conditions during emerald precipitation at Dyakou can be derived via the combination of the stable isotope thermometry and fluid source studies with the fluid inclusion isochores (Fig. 9). These constraints limit the formation of the emerald veins to approximately 365° to 420°C and pressures ranging from approximately 1,500 to 3,300 bars, corresponding to depths of 5 to 11 km. This may appear to be a large pressure range, but as this pressure range and likely the initial P-T uplift path roughly parallel the isochore trajectories, it should be noted that the pressure range at any specific temperature range is ±500 bars.

The derived range of pressure-temperature conditions and fluid compositions lies above the liquid-vapor curve for a saline brine (Sourirajan and Kennedy, 1962; Bodnar et al., 1985). This relatively distant position from the liquid-vapor curves indicates that precipitation of the emerald did not occur within a boiling system, nor are there any fluid inclusion assemblage observations indicative of boiling.

The fluid inclusion data are consistent with a range of salinities over relatively constant homogenization temperatures. This finding suggests fluctuating salinities driven by mixing of two relatively similar sources. The most likely scenario is that one fluid source is a brine related to the pegmatites and a second fluid is a local metamorphic fluid within the regional host rocks. A meteoric source is deemed unlikely as the emerald veins are relatively deep and the stable isotope data are consistent with magmatic and metamorphic sources and show no evidence of a meteoric signature.

TABLE 3. Hydrogen and Oxygen Stable Isotope Data

Sample no.	Mineral	$\delta D_{V\text{-}SMOW}$	$\delta^{18}O_{V\text{-}SMOW}$
DYK06-zh	Quartz		12.4
	Beryl		10.6
CH-EM-01	Beryl	–76.4	11.2

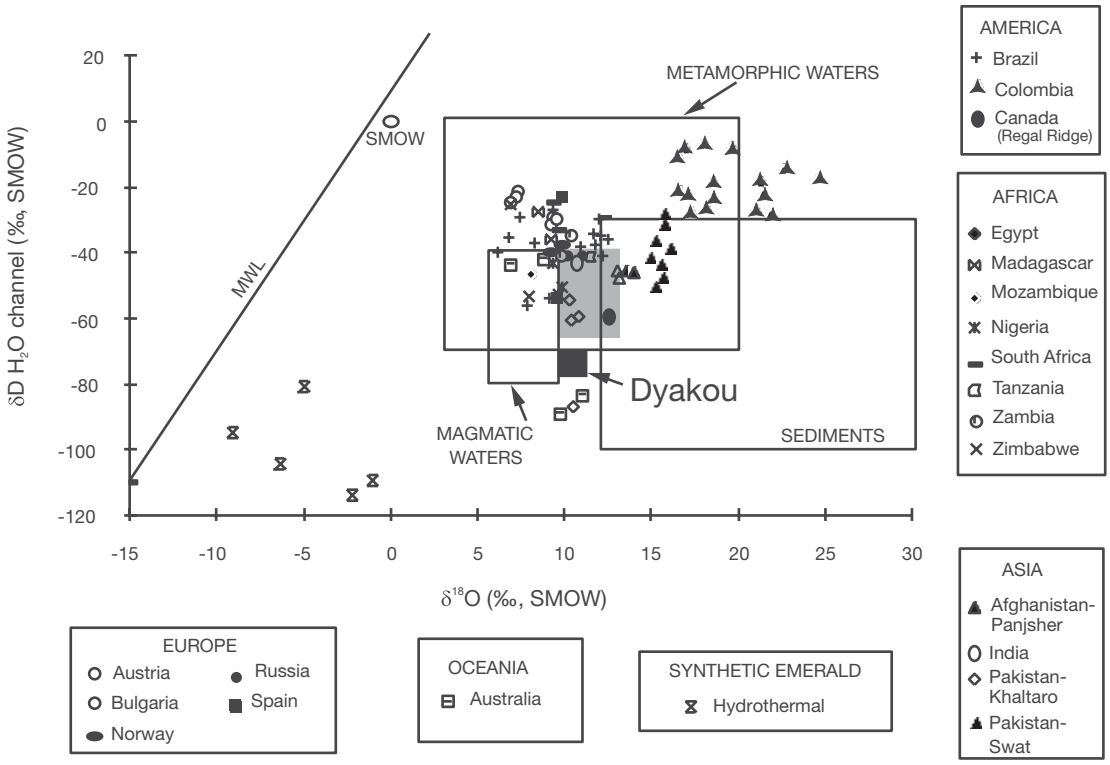

FIG. 8. Channel δD H_2O vs. calculated $\delta^{18}O$ H_2O (‰, SMOW) for emerald from emerald deposits (Giuliani et al., 1998; Groat et al., 2002). The Dyakou emerald $\delta^{18}O$ range is shown in black. The extended magmatic field for Cornubian (peraluminous) granites is shown in gray. The isotopic compositional fields are from Sheppard (1986).

Conclusions

Emerald at Dyakou is observed in quartz and quartz-pegmatite veins. Both vein types possess similar mineralogy, alteration, and fluid inclusion populations. ^{40}Ar-^{39}Ar evidence from muscovite and biotite from both vein types is consistent with a Cretaceous age for the emerald-bearing veins. These ages are consistent with a period of protracted suite of Cretaceous plutonism in this region (Feng et al., 1998; Yan et al., 2006; Liu et al., 2006) and that one of the plutons within this suite is likely responsible for the emerald mineralization at Dyakou.

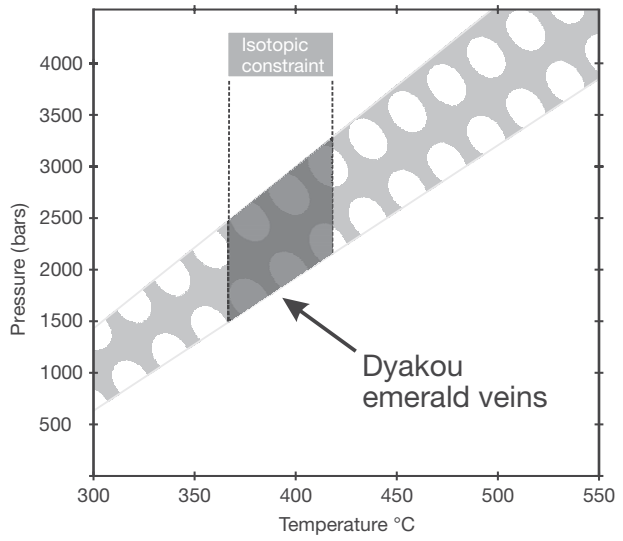

FIG. 9. Pressure-temperature diagram showing the derived constraints (black) for the Dyakou emerald veins derived from the intersecting areas of fluid inclusion isochore constraints (Swiss-cheese pattern) and stable isotope thermometry. Fluid inclusion isochores were derived using the isochore equations for saline brines of Bodnar and Vityk (1994).

Whole-rock geochemistry indicates that the Cretaceous intrusions are enriched in Be relative to the Saxi unit host rocks and that the host rock is enriched in Cr (±V) relative to other rock in the region. Thus the Cretaceous intrusions and the Saxi unit are the most likely sources of Be and Cr (±V) for the emerald.

The ^{18}O isotope thermometric results combined with the fluid inclusion isochores are consistent with vein formation at temperatures of 365° to 420°C and corresponding pressures of 1,500 to 3,300 bars in equilibrium with predominantly H_2O-NaCl brines ranging from 0.2 to 12.2 mass percent NaCl equiv. The δD-$\delta^{18}O$ data from individual emerald crystals are consistent with fluids derived from highly evolved granites.

Field relationships between the veins and host rocks, most notably the relatively high degree of regional metamorphic fabric within the host rocks and a corresponding lack of deformational fabric within the emerald-bearing veins, combined with the thermometry, stable isotopes, geochronology, and geochemistry are consistent with the Dyakou occurrence being an igneous-related emerald deposit, using the classification scheme of Schwarz and Giuliani (2001). A schematic of the relationship between the emerald-bearing veins and the associated rocks is shown in Figure 10.

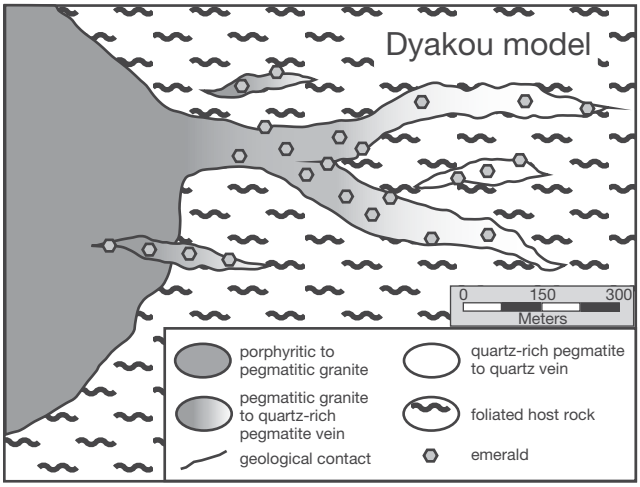

FIG. 10. Schematic showing the proposed relationships between the emerald-bearing quartz veins, the emerald-bearing quartz-rich pegmatite veins, the local Cretaceous porphyritic to pegmatitic granitic rocks, and the deformed Proterozoic host rocks.

Acknowledgments

Financial support for part of this project was provided by Natural Sciences and Engineering Research Council grants to DM, DT, and LG. Hu Rongrong from the Science and Technology University in Kunming, China, is gratefully acknowledged for assistance in the field. CFI and MFA grants to PCIGR at the University of British Columbia are acknowledged. Kerry Klassen from Queen's University is also gratefully acknowledged for oxygen isotope analyses of quartz and emerald. Two anonymous reviews and comments from R.J. Bodnar greatly improved an earlier version of this manuscript.

REFERENCES

Arif, M., Fallick, A.E., and Moon, C.J., 1996, The genesis of emeralds and their host rocks from Swat, northwestern Pakistan: A stable isotope investigation: Mineralium Deposita, v. 31, p. 255–268.

Beus, A.A., 1966, Geochemistry of beryllium: New York, Freeman, 401 p.

Bodnar, R.J., 1993, Revised equation and table for determining the freezing point depression of H_2O-NaCl solutions: Geochimimica et Cosmochimica Acta, v. 57, p. 683–684.

——2003, Introduction to fluid inclusions: Mineralogical Association of Canada Short Course 32, p. 1–8.

Bodnar, R.J., and Vityk, M.O., 1994, Interpretation of microthermometric data for H_2O-NaCl fluid inclusions, *in* De Vivo, B., and Frezzotti, M.L., eds., Fluid inclusions in minerals: Methods and applications: Blacksburg, VA, Virginia Tech., p. 117–130.

Bodnar, R.J., Burnham, C.W. and Sterner, S.M., 1985, Synthetic fluid inclusions in natural quartz. III. Determination of phase equilibrium properties in the system H_2O-NaCl to 1000°C and 1500 bars: Geochimimica et Cosmochimica Acta, v. 49, p. 1861–1873.

Feng, M.G., Lu, W., Zhang, X.G., Chen, G.F., and Zhang, S.T., 1998, Regional geologic mapping at 1:50,000 (Malipo and Dulong sheet): Yunnan, China, Yunnan Geological Survey Report F48E006011, 198 p.

Feng, M.G., Zhang, S.T., and Lu, W., 2000, Geological characters of the Chinese emerald deposit: Yunnan Geology, v. 19, p. 37–42.

Giuliani, G., France-Lanord, C., Zimmerman, J.L., Cheilletz, A., Arboleda, C., Charoy, B., Coget, P.,Fontan, F., and Giard, D., 1997, Fluid composition, δD of channel H_2O and $\delta^{18}O$ of lattice oxygen in beryls: Genetic implications for Brazilian, Colombian, and Afghanistani emerald deposits: International Geology Review, v. 39, p. 400–424.

Giuliani, G., France-Lanord, C., Coget, P., Schwarz, D., Cheilletz, A., Branquet, Y., Giard, D., Martin-Izard, A., Alexandrov, P., and Piat, D.H., 1998, Oxygen isotope systematics of emerald: Relevance for its origin and geological significance: Mineralium Deposita v. 33, p. 513–519.

Goldstein, R.H., and Reynolds, T.J., 1994, Systematics of fluid inclusions in diagenetic minerals: Society of Sedimentary Geology SEPM Short Course 31, 199 p.

Groat, L.A., Marshall, D.D., Giuliani, G., Murphy, D.C., Piercey, S.J., Jambor, J.L., Mortensen, J.K., Ercit, T.S., Gault, R.A., Mattey, D.P., Schwarz, D.P., Maluski, H., Wise, M.A., Wengzynowski, W., and Eaton, W.D., 2002, Mineralogical and geochemical study of the Regal Ridge showing emeralds, southeastern Yukon: Canadian Mineralogist, v. 40, p. 1313–1338.

Groat, L.A., Hart, C.J. R, Lewis, L.L., and Neufeld, H.L.D., 2005, Emerald and aquamarine mineralization in Canada: Geoscience Canada, v. 32, p. 65–76.

Hodges, K.V., and Spear, F.S., 1982, Geothermometry, geobarometry and the Al_2SiO_5 triple point at Mt. Moosilauke, New Hampshire: American Mineralogist, v. 67, p. 118–134.

Hoisch, T., 1991, Equilibria within the mineral assemblage quartz + muscovite + biotite + garnet + plagioclase and implications for the mixing properties of octahedrally-coordinated cations in muscovite and biotite: Contributions to Mineralogy and Petrology, v. 92, p. 413–427.

Leloup, P.H., Lacassin, R., Tapponnoier, P., Zhong, D., Liu, X., Zhang, L., Ji, S., and Phan Trong, T., 1995, The Ailao Shan-Red River shear zone (Yunnan, China), Tertiary transform boundary of Indochina: Tectonophysics, v. 251, p. 3–84.

Li, D.X., Deng, J., and Yang, X.Q., 1996, Metamorphic core complex and vortex structure in Laojunshan, southeastern Yunnan: Scientia Geologica Sinica, v. 5, p. 1–9.

Li, X.H, Li, Z.X., Zhou, H.W., Liu, Y., and Kinny, P.D., 2002a, U-Pb zircon geochronology, geochemistry and Nd isotopic study of Neoproterozoic bimodal volcanic rocks in the Kangdian rift of South China: Implications for the initial rifting of Rodinia: Precambrian Research, v. 113, p. 135–154.

Li, X.H., Li, Z.X., Zhou, H.W., Liu, Y., and Liang, X.R., 2002b, U-Pb zircon geochronological, geochemical and Nd isotopic study of Neoproterozoic basaltic magmatism in western Sichuan: Petrogenesis and geodynamic implications: Earth Science Frontiers, v. 9, p. 329–338.

Liu, Y.P., Ye, L., Li, C.Y., and Hu, R.Z., 2003, Laojunshan-Song Chay metamorphic core complex and its tectonic significance: Geochimica et Cosmochimica Acta, S1, A259.

Liu, Y.P., Ye, L., Li, C.Y., Song, B., Li, T.S., Guo, L.G., and Pi, D.H., 2006, U-Pb zircon SHRIMP geochronology and geochemical study of Neoproteroic magmatism in the Laojunshan area : Acta Petrologica Sinica, v. 22, p. 916–926.

Lu, W., Feng, M.G., and Hu, C.S., 2001, Metamorphism of the Mendong lithological group in the Nanwenhe area of southeast Yunnan: Yunnan Geology, v. 20, p. 25–33.

Maluski, H., Lepvrier, C., Jolivet, L., Carter, A., Roques, D., Beyssac, O., Tang, T.T., Nguyen, D.T., and Avigad, D., 2001, Ar-Ar and fission-track ages in the Song Chay Massif: Early Triassic and Cenozoic tectonics in northern Vietnam: Journal of Asian Earth Sciences, v. 19, p. 233–248.

Marshall, D., Groat, L., Giuliani, G., Murphy, D., Mattey, D., Ercit, T.S., Wise, M.A., Wengzynowski, W., and Eaton, W.D., 2003, Pressure, temperature and fluid conditions during emerald precipitation, southeastern Yukon, Canada: Fluid inclusion and stable isotope evidence: Chemical Geology, v. 194, p. 187–199.

Moroz, I., Roth, M., Sabot, B., Vapnik, Y., and Givan, A., 2004, Crystal chemistry and inclusions of Chinese emerald, *in* Pecchio et al., eds., Applied Mineralogy, p. 583–586.

Raase, P., 1974, Al and Ti contents of hornblende, indication of the pressure and temperature of regional metamorphism : Contributions to Mineralogy and Petrology, v. 45, p. 639–651.

Roger, F., Leloup, P.H., Jolivet, M., Lacassin, R., Phan, T.T., Brunel, M., and Seward, D., 2000, Long and complex thermal history of the Song Chay metamorphic dome (northern Vietnam) by multi-system geochronology: Tectonophysics, v. 321, p. 449–466.

Roedder, E., 1963, Studies of fluid inclusions. II: Freezing data and their interpretation: ECONOMIC GEOLOGY, v. 58, p. 167–211.

——1972, Composition of fluid inclusions: U.S. Geological Survey Professional Paper 440JJ, 164 p.

——1982, Fluid inclusions in gemstones: Valuable defects: International Gemological Symposium, Gemological Institute of America, Proceedings, p. 479–502.

Schwarz, D., and Giuliani, G., 2001, Emerald deposits—a review: Australian Gemologist, v. 21, p. 17–23.

Schwarz, D., Giuliani, G., and Grundmann, G., 2002, The origin of emerald: Geology and a classification of deposits, *in* Emeralds of the world: East Hampton, Lapis International, p. 18–23.

Sheppard, S.M.F., 1986, Characterization and isotopic variations in natural waters: Reviews in Mineralogy, v. 16, p. 165–183.

Sourirajan, S., and Kennedy, G.C., 1962, The system H_2O-NaCl at elevated temperatures and pressures: American Journal of Science, v. 260, p.115–141.

Tapponnier, P., Peltzer, G., and Armijo, R., 1986, On the mechanics of the collision between India and Asia: Geological Society [London] Special Publication 19, p. 115–157.

Tapponnier, P., Lacassin, R., Leloup, P.H., Scharer, U., Zhong, D., Liu, X., Ji, S., Zhang, L., and Zhong, J., 1990, The Ailao Shan/Red River metamorphic belt: Tertiary left-lateral shear between Indochina and South China: Nature, v. 343, p. 431–437.

Taylor, R.P., Fallick, A.E., and Breaks, F.W., 1992, Volatile evolution in Archean rare-element granitic pegmatites: Evidence from the hydrogen-isotopic composition of channel H_2O in beryl: Canadian Mineralogist, v. 30, p. 877–893.

Wang, H.Q., Zhang, S.T., Zhang, M.W., Lu, W., and Li, K.G., 1996, 1:10,000 geologic mapping at the Dyakou emerald showing: Yunnan, China, Yunnan Geological Survey Report, 33 p.

Wedepohl, K.H., 1978, Handbook of geochemistry: Berlin, Springer-Verlag.

Yan, D.P., Zhou, M.F., Wang, C.Y., and Xia, B., 2006, Structural and geochronological constrains on the tectonic evolution of the Dulong-Song Chay tectonic dome in Yunnan, SW China: Journal of Asian Earth Sciences, v. 28, p. 332–353.

Yang, Z.Y., and Besse, J., 1993, Paleomagnetic study of Permian and Mesozoic sediments from northern Thailand supports the extrusion model for Indochina: Earth and Planetary Science Letters, v. 117, p. 525–552.

Zhang, S.T., Feng, M.G., and Lu, W., 1998, Analysis of the Nanwenhe metamorphic core complex in southeastern Yunnan: Regional Geology of China, v. 17, p. 390–397.

Zhang, S.T., Feng, M.G., Wang, H.Q., Lu, W., and Yang, M., 1999, Geological features and genesis of emerald deposits in the Malipo County of Yunan Province, China: Geol. Sci. Tech. Info., v. 18, p. 50–54.

Zheng, Y.F., 1993, Calculation of oxygen isotope fractionation in hydroxyl-bearing silicates: Earth and Planetary Science Letters, v. 120, p. 247–263.